Electronic Supplementary Material (ESI) for Nanoscale.

Supplementary Information

Tuning Electronic Transport in Epitaxial Graphene-based van der Waals Heterostructures

Yu-Chuan Lin,[a] Jun Li,[b] Sergio C. de la Barrera,[b] Sarah M. Eichfeld,[a] Yifan Nie,[c] Rafik Addou,[c] Patrick C. Mende,[b] Robert M. Wallace,[c] Kyeongjae Cho,[c] Randall M. Feenstra,[b] and Joshua A. Robinson[a,*]

[a]Department of Materials Science and Engineering and Center for 2-Dimensional and Layered Materials, The Pennsylvania State University, University Park, PA 16802 USA

[b]Department of Physics, Carnegie Mellon University, Pittsburgh, PA 15213 USA

[c]Department of Materials Science and Engineering, The University of Texas at Dallas, Richardson, Texas 75080, USA

* E-mail: jrobinson@psu.edu

Methods	PV[1] WSe_2/EG	MOCVD WSe_2/EG (Sample 1)	MOCVD WSe_2/EG (Sample 2)
WSe_2 growth conditions	5 % H_2/Ar 5 -10 Torr 925 °C 30 mins.	100 % H_2 700 Torr 800 °C 30 mins.	100 % H_2 700 Torr 800 °C 30 mins.
C 1*s* of EG	284.1 eV	284.1 eV	284.1 eV
C 1*s* of EG after WSe_2 growth	284.4 eV (+ 0.3 eV)	284.0 eV (- 0.1 eV)	284.0 eV (- 0.1 eV)

Supplementary Table 1. Binding energy of C1*s*, which is corresponding to the C-C sp^2 from the epitaxial graphene (EG) used as template in powder vaporization (PV) and metal-organic chemical vapor deposition (MOCVD) for WSe_2 synthesis show the MOCVD process, carried out in a pure H_2 atmosphere, significantly shifts the C1*s* of WSe_2-EG towards a lower binding energy (This work, highlighted in the table). The C 1*s* of EG without exposure to WSe_2 synthesis is used as a reference.

$X_{EG_{PH}}$ (eV)	$X_{EG_{FH}}$ (eV)	$X_{WSe_2} + E_g$ (eV)	N_A (cm^{-2})	$N_{C,WSe_2-EG_{PH}}$ (cm^{-2})	$N_{C,WSe_2-EG_{FH}}$ (cm^{-2})
4.57	4.71	5.09	1.3×10^{12}	4.1×10^{5}	2.9×10^{12}
4.47	4.71	5.09	1.3×10^{12}	0.9×10^{4}	2.9×10^{12}
4.67	4.71	5.09	1.3×10^{12}	2.0×10^{7}	2.9×10^{12}
4.57	4.61	4.99	1.3×10^{12}	2.0×10^{7}	2.9×10^{12}
4.57	4.81	5.19	1.3×10^{12}	0.9×10^{4}	2.9×10^{12}

Supplementary Table 2. Computed dependence of electron affinity plus bandgap of WSe_2 ($X_{WSe_2} + E_g$), unintentional doping of WSe_2 (N_A), carrier density of WSe_2 after charge transfer between WSe_2 and EG_{PH} (N_{C,WSe_2-EGPH}), and carrier density of WSe_2 after charge transfer between WSe_2 and EG_{FH} (N_{C,WSe_2-EGFH}) on electron affinities of EG_{PH} ($X_{EG_{PH}}$) and EG_{FH} ($X_{EG_{FH}}$), respectively. An error range of $\pm$ 0.1eV for the input parameters is considered.

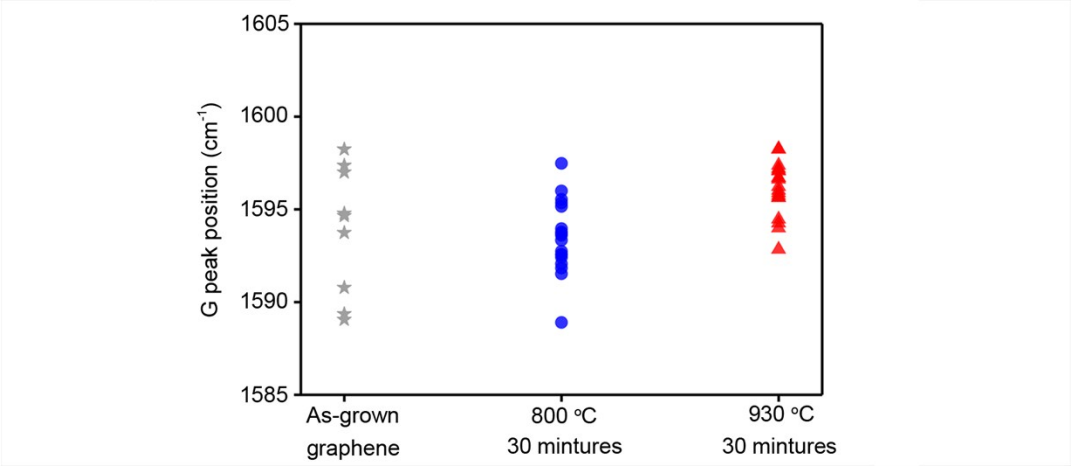

Supplementary Figure 1. The G peak positions from the same as-grown graphene and the graphene samples from the 800 °C and 930 °C WSe_2 growth that provide the information of the 2D peaks in the Figure 2 c and 2d.

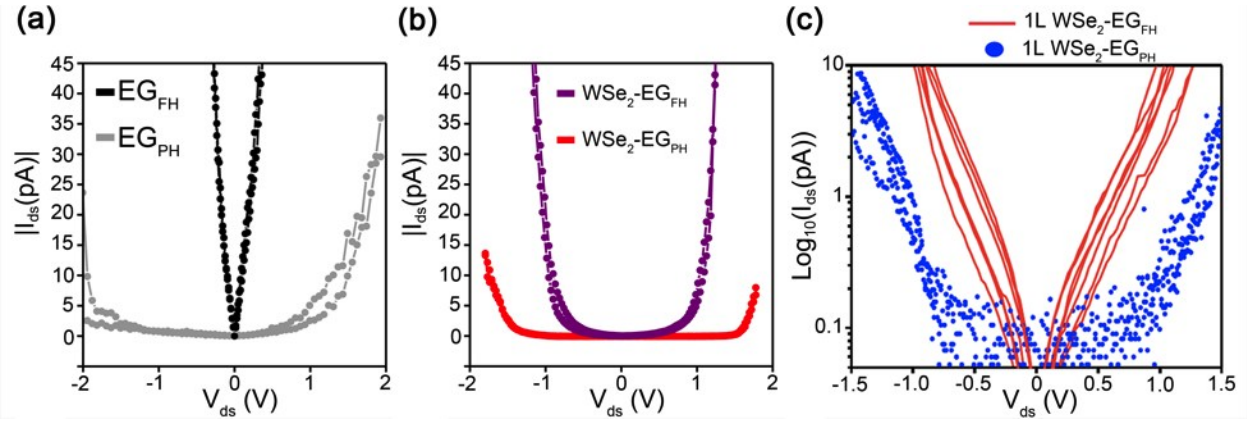

Supplementary Figure 2. (a) and (b) are linear plots of the I-V curves from graphene and WSe_2-graphene samples, respectively, presented in the Figure 4a. (c) A comparison of I-V curves measured on multiple 1L WSe_2 domains grown on EG_{PH} and EG_{FH} shows a clear reduction of turn-on voltage for the WSe_2-EG_{FH} case.

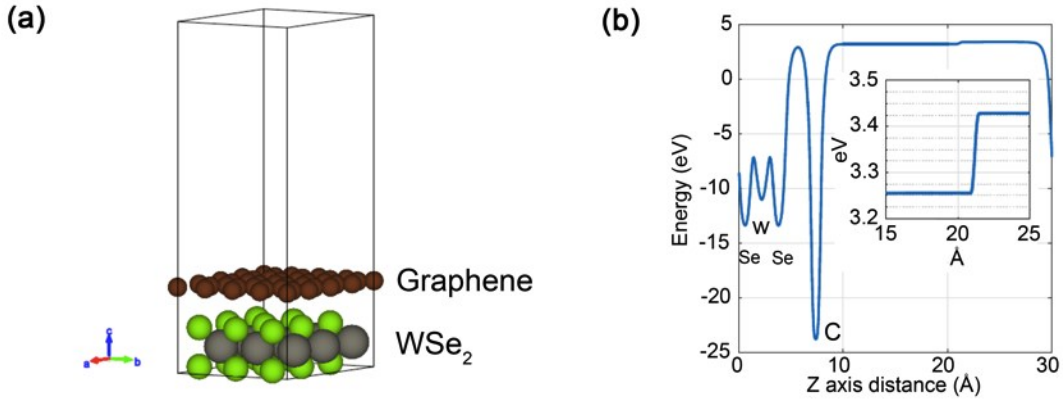

Supplementary Figure 3. (a) Plane averaged local electric potential energy of electrons along the stacking direction. (b) After dipole correction, a difference on vacuum energy above both sides of 0.17 eV is observed (zoomed inset).

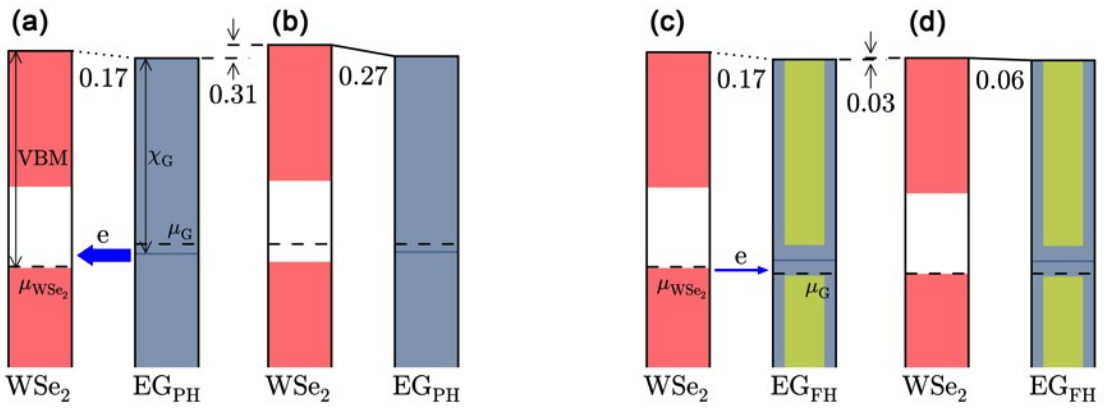

Supplementary Figure 4. Band alignment of WSe_2 and EG_{PH} (a) before charge transfer (including computed intrinsic dipole 0.17 eV), and (b) after charge transfer. Band alignment of WSe_2 and EG_{FH} (c) before charge transfer (including the intrinsic dipole), and (d) after charge transfer. Monolayer and bilayer graphene models are employed for EG_{PH} and EG_{FH} respectively, based on LEEM observations. Green shades in (c) and (d) represent conduction/valence subbands of bilayer graphene. The numerical values show various vacuum level differences, in units of eV.

Computational methods for the intrinsic dipoles between WSe_2 and graphene

The density functional theory (DFT) calculation are performed by Vienna ab-initio simulation package (VASP)[2] with the projector-augmented wave (PAW) method.[3] The local density approximation (LDA)[4] is used to describe the exchange-correlation functional with the partial core correction included. Spin polarization and spin-orbit coupling are applied. The stable phase of the monolayer WSe_2 is trigonal prism structure.[5] The optimized planar lattice constant of WSe_2 is 3.25Å, and the optimized planar lattice constant for monolayer graphene is 2.45 Å. In order to fit the lattice constant, a super cell with 3×3 WSe_2 unit cells and 4×4 graphene unit cell is used, and a compressive strain of 0.4 % is applied to graphene, as the electronic behaviors of TMD are very much susceptible to lattice strain. The super cell is shown in Figure 2a. The wave functions are expanded in plane waves with a kinetic energy cutoff of 500 eV, and the convergence criteria for the electronic relaxation is 10^{-5} eV. Integration over the Brillouin zone is performed with a gamma-centered 6×6×1 Monkhorst-Pack k-point mesh for ionic and electronic optimization. A vacuum region of about 15Å normal to the surface is added to minimize the interaction between adjacent slabs (Figure S3a). Dipole correction on the stacking direction is used in systems to reveal the dipole within the two layers caused by the Fermi-level alignment. The local density approximation (LDA) is found to be suitable for studying the metal-TMD contact.[6] The generalized gradient approximation (GGA)[7] with the DFT-D2 method for van der Waals (vdW) corrections[8] is also used to cross-check the structural accuracy. We find that GGA results with vdW corrections are in overall agreement with LDA results. Both the LDA method and the GGA+vdW method result in a similar

structure with a distance of ~3.5 Å between graphene and TMD, indicating a secondary bond interaction. The energy difference between the vacuum regions on the both sides of the contact system is the dipole induced by the contact. The vacuum energy level above WSe_2 is 0.17 eV higher than that above graphene, indicating a dipole from graphene towards the WSe_2 (Figure S3b).

Computation of WSe_2 doping density and charge densities, and dependence on parameters

For the computation of charge transfer and band alignment, we take the doping densities of EG_{PH} and EG_{FH} from our experimental values, as discussed in the main text. Parameters in the computation are the electron affinities for monolayer and bilayer graphene, with nominal values of 4.57 eV and 4.71 eV, respectively, as known from prior experiments.[9] We take the sum of the electron affinity plus band gap of the WSe_2, $\chi_{WSe_2} + E_g$, to be an unknown in the computation, since a value for this sum is not accurately known from prior work (only the sum is considered here since the electron occupation in the conduction band of the WSe_2 is negligible). A second unknown is the unintentional doping density of WSe_2. Then, using the two measured work function differences for WSe_2 on both EG_{PH} and EG_{FH} compared to the bare EG_{PH} and EG_{FH}, we can determine values for the two unknown parameters. The carrier densities for the WSe_2 on both EG_{PH} and EG_{FH} after charge transfer are then a byproduct of the computation. Table S2 shows dependence of these quantities on the input parameter values. In all cases, the carrier densities of WSe_2 in WSe_2-EG_{PH} are very much greater than those of WSe_2 in WSe_2-EG_{FH}, consistent with the observed differences in the CAFM I-V results.

We note that the doping density values in Table S2 are all the same, reflecting a tight constraint on this value. This constraint arises from charge transfer between the WSe_2 and the EG_{PH}. As pictured in Figure S4a and 4b, since the Fermi energies of the EG_{PH} and WSe_2 are relatively far apart prior to charge transfer, and hence the Fermi energy of the WSe_2 ends up well within its band gap after the transfer, then the p-type doping density in the WSe_2 is directly determined by the doping density of the EG together with the difference between the electron affinity of the EG_{PH} and the $\chi_{WSe_2} + E_g$ value of the WSe_2. The resulting carrier densities for the WSe_2 on EG_{PH} are negligible, again since the resulting WSe_2 Fermi energy is well within the gap. On the other hand, for the WSe_2 on EG_{FH}, their Fermi energies are relatively close prior to charge transfer, as pictured in Figure S4c and 4d. The resulting Fermi energy for the WSe_2 on EG_{FH} ends up near or within the valence band even after the charge transfer, with concomitant large carrier density, and the value of the WSe_2 doping density is not so tightly constrained in this part of the problem.

We have also considered the effect on the computed carrier densities of variation in the EG_{PH} and EG_{FH} doping density values, as well as variation of the measured work functions differences within their experimental error ranges. Doping densities of $(4 \pm 1) \times 10^{12}$ cm^{-2} for EG_{PH} and $(1.5 \pm 0.2) \times 10^{13}$ cm^{-2} for EG_{FH} are typical measured in our samples. Considering the variations of these doping densities, the carrier density of WSe_2 on EG_{FH} after charge transfer is computed to range from $2.5 - 3.0 \times 10^{12}$ cm^{-2} while the carrier density of WSe_2 on EG_{PH} after transfer is always less than 10^7 cm^{-2}, i.e. its Fermi is well within the bandgap. For the measured error ranges ($\pm$0.03 eV) on the work function differences, performing computations at the bounds of these values produces carrier densities in the WSe_2 on EG_{FH} compared to WSe_2 on EG_{PH} that continue to differ by more than a factor of 10^4, for all cases.

Reference:

1 Y.-C. Lin, R. K. Ghosh, R. Addou, N. Lu, S. M. Eichfeld, H. Zhu, M.-Y. Li, X. Peng, M. J. Kim, L.-J. Li, R. M. Wallace, S. Datta and J. A. Robinson, *Nat. Commun.*, 2015, **6**, 7311.

2 G. Kresse and J. Furthmüller, *Phys. Rev. B*, 1996, **54**, 11169–11186.

3 G. Kresse and D. Joubert, *Phys. Rev. B*, 1999, **59**, 1758–1775.

4 D. M. Ceperley and B. J. Alder, *Phys. Rev. Lett.*, 1980, **45**, 566–569.

5 C. Gong, H. Zhang, W. Wang, L. Colombo, R. M. Wallace and K. Cho, *Appl. Phys. Lett.*, 2013, **103**, 053513.

6 C. Gong, L. Colombo, R. M. Wallace and K. Cho, *Nano Lett.*, 2014, **14**, 1714–20.

7 J. P. Perdew, K. Burke and M. Ernzerhof, *Phys. Rev. Lett.*, 1997, **78**, 1396–1396.

8 G. Makov and M. Payne, *Phys. Rev. B*, 1995, **51**, 4014–4022.

9 Y.-J. Yu, Y. Zhao, S. Ryu, L. E. Brus, K. S. Kim and P. Kim, *Nano Lett.*, 2009, **9**, 3430–3434.